A&A 505, 755–762 (2009)
DOI: 10.1051/0004-6361/200811374
© ESO 2009

Astronomy & Astrophysics

The X-ray spectrum of the classical TTauri star TW Hydrae observed by *LETGS* aboard *Chandra*

A. J. J. Raassen[1,2]

[1] SRON Netherlands Institute for Space Research, Sorbonnelaan 2, 3584 CA Utrecht, The Netherlands
[2] Astronomical Institute "Anton Pannekoek", Kruislaan 403, 1098 SJ Amsterdam, The Netherlands
e-mail: a.j.j.raassen@sron.nl

Received 18 November 2008 / Accepted 27 July 2009

ABSTRACT

Aims. I present the analysis of the X-ray spectrum of the classical TTauri star TW Hydrae, and determine emission measure distributions, elemental abundances, electron temperatures, densities, and line fluxes.

Methods. TW Hya was observed in the wavelength range 5–175 Å by *CHANDRA-LETGS*. I performed a multi-temperature fit, based on a collisional ionisation equilibrium (CIE) model for optically thin plasmas. I measured line fluxes by fitting a Gaussian line profile, folded through the response matrix, to the observed line features and I applied these values to establish plasma properties.

Results. No line features were established in the spectrum above 40 Å. Due to the absence of line features above 40 Å $N_{\rm H}$ is calculated to be somewhat higher than assumed so far. The observed "coronal" temperature covers a range from about 1.5 to 20 MK. The abundance pattern shows a very strong enhancement of Ne and some enhancement of N. From forbidden-intercombination line ratios of O VII and of Ne IX I obtain a value for the electron density of $n_{\rm e} \simeq 10^{12}$ cm^{-3}. This is higher than the value for electron densities in coronal plasmas of older late type main-sequence stars. A blackbody component was added to describe the shape of the continuum around 15 Å better. The emitted X-ray luminosity is in the order of 10^{30} erg/s.

Key words. techniques: spectroscopic – stars: individual: TW Hya – stars: coronae

1. Introduction

TTauri stars (TTS) are young low-mass pre-main sequence stars, especially present in star-forming regions. They can be divided into two types: classical TTauri stars (cTTS) and weak-line TTauri stars (wTTS). Different from the cTTS, the weak-line TTauri stars do not show strong H_α emission. Classical TTauri stars are surrounded by a disc of gas and dust, while the weak-line TTauri stars have no surrounding disc. Both types of TTauri stars are X-ray emitters. The X-rays were observed by the Einstein Satellite (e.g. Feigelson & DeCampli 1981) and by ROSAT (e.g. Feigelson et al. 1993). The X-rays from weak-line TTauri stars are commonly interpreted as being produced by a scaled up coronal structure. The same is true for classical TTauri stars. However, in cTTS additional mechanisms might be present e.g., jets, winds, or accretion from the disc to the stellar surface. In the last case it is expected that the material funnels from the disc to the stellar surface along magnetic field lines, resulting in hot X-ray emitting spots. TW Hya belongs to the group of classical TTauri stars. It is spectral type K8V (SIMBAD) and nearby, at a distance of 56.4 parsec (Perryman et al. 1997a, b), recently corrected to 53.7 parsec (van Leeuwen 2007). It is surrounded by a circumstellar disc. A wide range of periods has been given over the years (e.g., Herbst & Koret 1988; Mekkaden 1998; Rucinski et al. 2008). Recently, Setiawan et al. (2008) have concluded that a Jupiter-like planet is present close to the star, inside the disc and with a period of 3.56 days. However, Huélamo et al. (2008) state that a cool spot on the stellar surface is more likely to explain the observations.

Since the era of high-resolution X-ray spectroscopy started after the launches of *Chandra* and *XMM-Newton*, many papers on the high-resolution X-ray spectrum of TW Hya have appeared. The *RGS* aboard *XMM-Newton* was used by Stelzer & Schmitt (2004) and Robrade & Schmitt (2006), while *HETGS* aboard *Chandra* was applied by Kastner et al. (2002) and Ness & Schmitt (2005). Robrade & Schmitt (2006) and Stelzer & Schmitt (2004) made a fit to the spectrum with three temperature bins, while Stelzer & Schmitt (2004), Kastner et al. (2002), and Ness & Schmitt (2005) investigated individual lines and line fluxes. Güdel & Telleschi (2007) studied the O VII/O VIII line ratio in an ensemble of wTTS and cTTS.

For *RGS* and *HETGS* the wavelength ranges are at the higher end limited to about 35 Å. Applying *LETGS*, however, I may extend the wavelength range to far higher wavelengths and check the effects of the models above the *RGS* and *HETGS* limits.

The strategy in this paper is to perform a multi-temperature fit to the total spectrum (Sect. 3). In this fitting procedure firstly two different models have been applied (CIE and NEI) and the optimal number of T-components has been determined. Results of the global fitting are compared with results from the analysis based on individual lines, described in Sect. 4. In Sect. 5 I discuss the agreements and differences in comparison with the papers mentioned above (Robrade & Schmitt 2006; Stelzer & Schmitt 2004; Kastner et al. 2002; and Ness & Schmitt 2005).

2. Observations

The spectrum of TW Hya was obtained on August 22, 2006 during a 151.64 ks observation using HRC-S in combination with

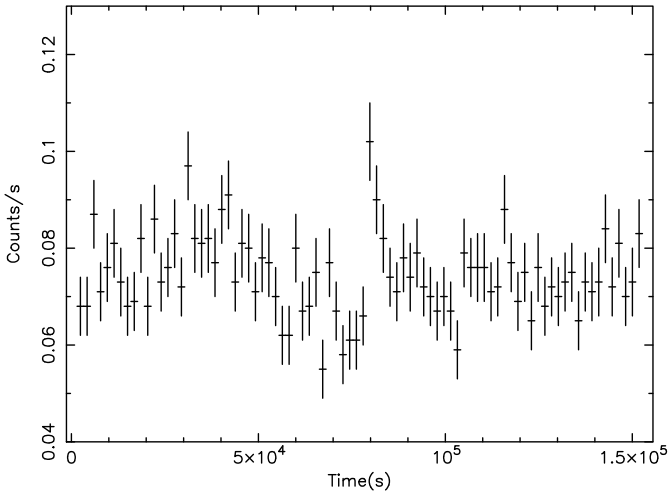

Fig. 1. The zeroth order lightcurve of the *LETGS* observation of TW Hya. The time bin size is 1800 s.

Table 1. Observation log of the data of TW Hya.

Obs ID	Instrument	Grating	Start Date	Exp.(ks)
6443	HRC-S	LETG	2006-08-22T07:47:56	151.64

LETG aboard *CHANDRA*. The log of the observations is shown in Table 1. The data were pipelined with CIAO3.4 with CALDB version 3.4.2 and prepared to be implemented in SPEX by the programs *extract* and *crele* developed at SRON.

In the lightcurve based on the total detector area some time bins showed saturation, i.e., they registered over 184 counts/s. Although this saturation will only sparely influence the spectral counts, the saturated time bins were excluded from the further procedure. Figure 1 shows the zeroth order lightcurve. The time bin size is 1800 s. The average count rate is 0.07 counts/s. This lightcurve shows variability up to about 50% over the total exposure time. However, no specific time intervals could be selected to obtain a reliable spectrum of a "flare" state. No periodicity was established during the observation.

The observed *LETGS* spectrum covers the range from 1 to 176 Å. The final spectrum is the result of the sum of the spectrum of the +1 order and the −1 order. The background, which is high at longer wavelengths, was subtracted. No significant line features (apart from higher order lines) are established above 40 Å.

3. Multi-temperature fitting

3.1. A 10-T CIE and NEI model as a starter

I started the analysis of the *LETGS*-spectrum of TW Hya by means of two different spectral models: a model for optically thin plasma in collisional ionisation equilibrium (CIE) and a model for a non-equilibrium plasma (NEI). This approach was chosen to investigate the possibility of establishing different mechanisms for hot X-ray radiation i.e., a coronal part as for the wTTS and an accretion part from in-falling disc material. The two different models resulted in a solution with three significant temperature components only and with comparable χ^2 values. However, the parameter $U(=n_e \times t)$ in the NEI model obtained a value that high that equilibrium is reached and the NEI model mimics the CIE model.

From this point on I use a 3-T model for optically thin plasma in collisional ionisation equilibrium (CIE) as implemented in SPEX version 2.0[1] (Kaastra et al. 1996a) in combination with MEKAL (Mewe et al. 1995; Kaastra et al. 1996b). The ionisation equilibrium is based on calculations by Arnaud & Rothenflug (1985).

3.2. A 3-T model

A 3-T model was fitted to the data over the total wavelength range from 5 to 175 Å. The T-parameters, emission measures and abundances were freely varied. Two temperature components, describing most of the line features, are established at 0.127 keV and 0.264 keV. They describe very well the observed line structure above 10 Å. Based on the Mg XI, Mg XII and Si XIII, Si XIV line features below 10 Å a third temperature component at 1.45 keV is determined. A fourth T-component of 0.65 keV appeared to model the continuum. These components are in agreement with the temperatures found by Robrade & Schmitt (2006) and Stelzer & Schmitt (2004) in a different way and based on observations with *RGS* on board of *XMM-Newton*.

However, fitting the spectrum with these four CIE components results in some deviations, i.e., the model continuum is a bit lower than the data around 15 Å and a bit higher below 10 Å, while weak line features below 10 Å are not recognised as lines by the model. I notice the same deviations when applying the parameter set given by Robrade & Schmitt (2006). To solve this deficiency in the shape of the underlying continuum around 15 Å, a blackbody component was introduced, replacing the $T = 0.65$ keV component. The blackbody component has a well determined temperature of 0.187 keV, just in between the two cool temperature components. This component is strongly related to the 0.60 keV temperature component of Robrade & Schmitt (2006), but doesn't affect the other T-components. From Table 2 of Günther et al. (2007) we notice that the CIE component at 0.7 keV doesn't improve their fit very significantly. The blackbody component improved the shape of the continuum and it lowered the χ^2 of the fit significantly. Due to the lower continuum below 10 Å the weak line features appear more pronounced. It results in a higher value of the abundance of Si, compared to the value given by Robrade & Schmitt (2006). It is possible that my blackbody component takes into account many weak lines, that are not included in the models and produce a pseudo-continuum.

The spectrum and the model are shown in Fig. 2. The grey line (green in the electronic version) is the model fit to the spectrum.

The parameter values of the fit are collected in Table 2. This table shows the interstellar column density N_H, the determined temperature values, the emission measures and the emitted luminosities of the different temperature bins, the electron densities, and the abundances. The emission measure is defined as $EM = n_e n_H V$, in which $N_H = 0.85 \times n_e$. Except for the density, broadening, and w-shift, the parameters were all fitted simultaneously.

The interstellar column density N_H was free to vary. Only one N_H parameter was used for all four components. However, it is not necessarily true that all plasma undergoes the same absorption. The continuum at higher wavelength is weak and

[1] http://www.sron.nl/~divisions/hea/spex/version2.0

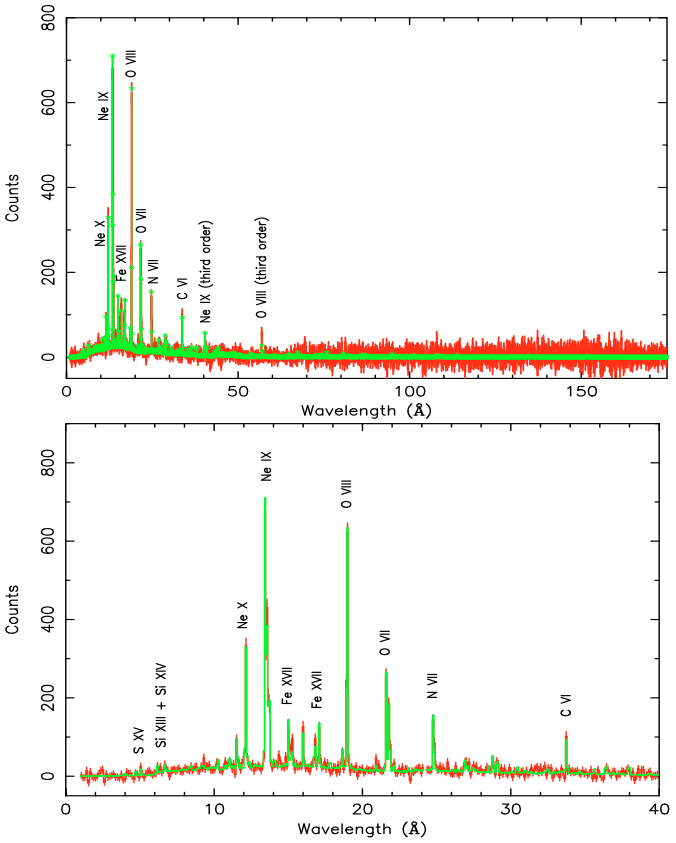

Fig. 2. The *LETGS* spectrum of TW Hya together with the fitted CIE model, grey line (green in the electronic version). *The top panel* shows the total spectrum and *the bottom panel* shows the area between 0 and 40 Å.

Table 2. Parameters of the 3-T fit to the spectrum of TW Hya.

Parameters		
$\log N_{\rm H}$[cm^{-2}]	20.72(.09)	
distance	53.7 pc	
w-shift	1.2e-4	
broadening	287 km s^{-1}	
T_1[keV]	0.127(.012)	
T_2[keV]	0.264(.007)	
T_3[keV]	1.45(.43)	
$T_{\rm Bb}$[keV]	0.187(.016)	
EM_1[10^{51}cm^{-3}]	11.5(3.3)	
EM_2[10^{51}cm^{-3}]	26.3(2.1)	
EM_3[10^{51}cm^{-3}]	9.3(2.5)	
$Area_{\rm Bb}$[10^8cm^2]	3.57(1.7)	
$n_{\rm e}$O VII[10^{11}cm^{-3}]	6.3(2.6)	
$n_{\rm e}$Ne IX[10^{12}cm^{-3}]	2.5(0.4)	
$L_{\rm X1}$[10^{30}erg/s][a]	0.14(.04)	
$L_{\rm X2}$[10^{30}erg/s]	0.83(.07)	
$L_{\rm X3}$[10^{30}erg/s]	0.29(.08)	
$L_{\rm Bb}$[10^{30}erg/s]	0.43(.20)	
$L_{\rm Tot}$[10^{30}erg/s]	1.69(.22)	
		A/O
C	1.26(.23)	1.26(.24)
N	2.87(.31)	2.87(.33)
O	1.00(.04)	1.00(.06)
Ne	10.3(.34)	10.3(.53)
Mg	1.61(.89)	1.61(.89)
Si	1.35(.43)	1.35(.43)
Fe	0.61(.06)	0.61(.06)
Ni	0.70(.49)	0.70(.49)
χ^2/d.o.f.	1564/1536	
$\chi^2_{\rm red}$	1.02	

Notes: Statistical 1σ errors are in parentheses. The emitted luminosity ($L_{\rm X}$) is given in the range from 0.3 to 10 keV.

not very reliable due to the high value of the subtracted background. However, line features or the absence of line features are indicative for the interstellar column density. The absence of the Ne VIII lines around 88 and 98 Å indicates a value for $N_{\rm H} \geq 2 \times 10^{20}$ cm^{-2}. My fitted value ($N_{\rm H} = 5.2 \times 10^{20}$ cm^{-2}) is higher than that value and also slightly higher than the values used by Robrade & Schmitt (2006) and Stelzer & Schmitt (2004). This higher value is necessary to suppress Si XII line features near 44 Å that appear in the model, but are absent in the observed spectrum. These lines are outside the wavelength range observed by Robrade & Schmitt (2006) and Stelzer & Schmitt (2004).

A slight shift in λ (≈1.2e-4) was applied to optimise the positions of the model lines with respect to the data. This shift corresponds to about 35 km s^{-1}. The value of $v_{\rm rad}$ of TW Hya is 12.5 km s^{-1} (Reid 2003), while the satellite and earth orbital motion result in about −12 km s^{-1} at time of observation. My fitted value is higher than the result of these geometrical motions. An instrumental wavelength calibration bias is likely on forehand and cannot be ruled out.

A line broadening parameter, which corresponds to a velocity broadening of 287 km s^{-1}, was added to improve the fit. This parameter is added to the instrumental line spread function, which is taken into account by means of folding the model with the response matrix. Ness & Schmitt (2005) obtain the best fit results by introducing an *FWHM* of 0.016 Å for all lines of their *HETGS* observation. This is equivalent to about 200 km s^{-1}. They do not mention whether this broadening is included with the instrumental broadening or not.

The densities given in Table 2 are obtained by fitting to the line triplets of He-like ions (see also Sect. 4.3) in a narrow selected wavelength range around 22 Å (O VII) and around 13.5 Å (Ne IX) only. During this fit procedure the oxygen and neon abundances and electron density ($n_{\rm e}$) were free to vary, while all other parameters were fixed at values obtained in the overall fitting procedure. The abundance served as normalisation parameter. The obtained electron densities are $n_{\rm e} = 6.3(2.6) \times 10^{11}$ cm^{-3} based on the O VII line triplet and $n_{\rm e} = 2.5(0.4) \times 10^{12}$ cm^{-3} based on Ne IX.

The emitted luminosities are calculated over the energy range from 0.3 to 10 keV. They are obtained for all given temperature bins. The uncertainty in the luminosities is assumed to be the same as the relative uncertainties of the emission measures. Robrade & Schmitt (2006) and Stelzer & Schmitt (2004) give luminosity values in slightly different energy ranges. In their energy ranges, 0.2–10 keV and 0.45–2.25 keV, respectively, they obtain 2.0×10^{30} erg/s and 1.4×10^{30} erg/s. The luminosities in these ranges obtained in the model fit of this study (corrected for the distance they use) are 2.05×10^{30} erg/s and 1.47×10^{30} erg/s, respectively. They are in very good agreement with those of Robrade & Schmitt (2006) and Stelzer & Schmitt (2004). It shows that the luminosity is a very robust quantity. About 55% of the emitted luminosity is due to line radiation,

while the resulting 45% is radiated in the continuum or a pseudo-continuum produced by many weak indistinguishable lines not present in the models. These percentages are comparable with values (60% versus 40%) obtained using the parameter set of Robrade & Schmitt (2004).

The abundances are coupled for the three temperature components. This is done to stabilise the fit procedure and is not based on physical grounds. The abundances are relative to solar photospheric values (Anders & Grevesse 1989), except for iron. For Fe the value of Grevesse & Sauval (1999) has been applied. It differs by a factor 1.45. For the obtained abundances the over-abundance of neon (a factor of ten higher than oxygen) is most remarkable, while the abundance of nitrogen is a factor 3 higher in comparison with oxygen. The other abundances are close to solar. Iron seems to be depleted. My absolute abundance values are far higher than values given by Stelzer & Schmitt (2004). This can be explained by the fact that the abundances are strongly anti-correlated with the emission measures. Therefore in many papers an abundance ratio related to the abundance of an arbitrarily chosen, generally dominantly present element is given. The abundance pattern, i.e., abundances relative to oxygen (A/O), agrees very well with the results of Stelzer & Schmitt (2004). My carbon abundance is somewhat higher as a result of my higher $N_{\rm H}$ value. The quantity $A \times EM$ is robust. My values for the emission measures are far lower than those in the paper by Stelzer & Schmitt (2004). However, the ratio between the EM_2 and EM_1, given by them as 2.35, is the same as in my fit i.e., 2.36.

The errors given in the paper are quite different for different quantities. The T parameters, emitted luminosities, abundance ratios (A/O), the observed line fluxes, and $A \times EM$, given in Sect. 4 are robust. Their statistical 1σ errors given in Tables 2–4 are robust. For the abundances and the emission measures, however, the errors given in Table 2 are statistical errors that belong to the given fit-parameters. The absolute values of the abundance and emission measures might change considerably more as long as the abundance ratios (A/O) and $A \times EM$ remain unchanged.

4. Individual line fluxes

The individual observed line photon fluxes of the *LETGS* spectrum of TW Hya have been measured. Many line features are located between 10 and 25 Å. Unfortunately, the number of line features above 40 Å are scarce. The most obvious features above 40 Å are higher order lines of oxygen and neon. Lines below 10 Å are weak, but definitely present, as they are well positioned in relation to experimental laboratory wavelengths in databases (Kelly 1987, and NIST[2]).

For each observed line a Gaussian profile was folded through the response matrix and fitted to the line feature together with a power-law taking into account for the continuum. For lines used for the temperature and density determination in Sect. 4.3 also the following (maybe more sophisticated) method was applied. This was done to avoid contributions by blends. After the final overall multi-temperature fit (Sect. 3.2), the three wavelength ranges that belong to He-like ions (28.5–29.8 Å for N VI), (21.4–22.4 Å for O VII, and 13.2–14 Å for Ne IX) were selected. Then the ions N VI, O VII, and Ne IX were ignored from the model. Now the model describes the total spectrum except the He-like line triplet of the ignored ions. These lines were measured by folding a Gaussian through the response matrix and by fitting to the lines, as described in Sect. 4, but without the additional power-law, since the continuum is taken into account by the multi-temperature model. During this fit all parameters of the model were fixed, except the Gaussians. This way the positions, observed photon fluxes, and widths (*FWHM*) of the lines were established. Thanks to the folding of the Gaussian profile through the response matrix and the Line-Spread-Function (LSF) the given *FWHM* are net values, in addition to the instrumental width. The measured wavelengths, widths and line photon fluxes are collected in Table 3 together with the theoretical wavelengths from laboratory measurements (Kelly 1987).

Especially at higher wavelengths the lines are slightly shifted to longer wavelength. Unfortunately the line features do not extent to wavelengths above 40 Å. An underlying instrumental wavelength imperfection, cannot be ruled out. However, all lines given by Stelzer & Schmitt (2004) in their Table 2, based on observations with *RGS*, are (even more pronounced) shifted to longer wavelengths, albeit they do not report this shift and

[2] http://physics.nist.gov/PhysRefData/ASD/index.html

Table 3. The observed line photon fluxes.

ion	λ_0 [Å]	$\lambda_{\rm obs}$ [Å]	*FWHM* [Å]	Observed flux
S XV	5.064	5.061(.035)	—	16.6(11.8)
Si XIV	6.182	6.200(.018)	—	3.9(2.3)
Si XIII	6.648	6.656(.023)	—	3.4(2.2)
Si XIII	6.688	6.698(.041)	—	2.4(2.2)
Si XIII	6.740	6.766(.027)	—	2.7(2.2)
Mg XII	8.423	8.474(—-)	—	4.2(—-)
Mg XI	9.169	9.168(.014)	—	6.4(3.4)
Mg XI	9.315	9.318(.018)	—	12.0(6.2)
Ne X	9.708	9.689(.032)	—	7.6(4.8)
Ne X	10.239	10.225(.011)	—	11.5(4.5)
Ne IX	10.765	10.759(.012)	—	7.7(3.7)
Ne IX	11.001	10.994(.008)	—	12.6(4.2)
Ne IX	11.544	11.543(.006)	—	22.0(4.8)
Ne X	12.134	12.135(.003)	0.017(.014)	89.6(7.8)
Ne IX	13.447	13.452(.002)	0.024(.007)	215.0(11.0)
Ne IX	13.553	13.555(.002)	$\lesssim$0.020	129.0(9.0)
Ne IX	13.700	13.699(.003)	0.041(.011)	81.2(7.7)
Ni XIX	14.040	14.058(.028)	$\lesssim$0.093	5.6(4.4)
Ni XVIII	14.081			
Ni XVIII	14.370	14.381(.033)	$\lesssim$0.120	10.2(6.6)
O VIII	14.821	14.824(.014)	—	6.9(2.8)
Fe XVII	15.013	15.031(.008)	0.070(.022)	35.9(6.5)
O VIII	15.176	15.174(.020)	fix	9.0(4.1)
Fe XVII	15.260	15.258(.008)	$\lesssim$0.056	17.4(5.1)
O VIII	16.006	16.010(.006)	$\lesssim$0.053	29.7(5.4)
Fe XVII	16.775	16.790(.006)	$\lesssim$0.041	20.4(4.6)
Fe XVII	17.051	17.056(.060)	fix at 0	22.9(12.6)
Fe XVII	17.100	17.098(.039)	fix at 0	15.1(10.3)
O VII	18.627	18.634(.018)	0.066(.060)	17.5(6.7)
O VIII	18.969	18.972(.002)	0.027(.006)	229.0(12.0)
N VII	20.910	20.917(.019)	0.069	20.7(8.6)
O VII	21.602	21.610(.003)	$\lesssim$0.043	119.0(12.0)
O VII	21.804	21.807(.003)	0.030(.011)	103.0(11.0)
O VII	22.101	22.105(.015)	0.035	15.3(6.3)
N VII	24.781	24.794(.005)	0.046(.018)	81.2(11.3)
N VI	28.787	28.799(fix)	0.138(.103)	31.2(12.0)
N VI	29.084	29.096(fix)	$\lesssim$0.146	27.1(10.0)
N VI	29.536	29.548(fix)	—	6.0(6.3)
C VI	33.736	33.743(.005)	—	59.3(11.0)

Notes: Statistical 1σ errors are in parentheses. λ_0 is the theoretical wavelength from Kelly (1987). $\lambda_{\rm obs}$ is the observed wavelength. The flux is in units 10^{-6} photons cm^{-2} s^{-1}.

they do not give error estimates for their wavelength measurements. Moreover, Günther & Schmitt (2008) measure positive line shifts of the same order of magnitude, based on observations with *FUSE* and *HST* (see their Tables 4 and 5). It should be kept in mind that these observations concern another wavelength area and lower stages of ionisation. Therefore they might be related to other physical processes. The observed wavelength shift in the X-ray regime seems to be real. If not from physical origin, the observed shift would imply a calibration issue for both instruments (*LETGS* and *RGS*).

For a number of lines an *FWHM* could be obtained. However, the line widths are in many cases upper limits. The *FWHM* of a line can be linked to a velocity (v) by the formula: $FWHM(\text{Å})/\lambda_{\rm obs} = 2\sqrt{\ln 2}v/c$. Applying this formula to the stronger isolated lines at 13.447 Å, 18.969 Å, 21.602 Å, and 24.781 Å, I obtain values for v of 321(94), 256(57), $\lesssim$358, and 334(130) km s^{-1}, respectively. In Sect. 3.2 I have obtained an overall broadening parameter (v = 287 km s^{-1}) to improve the multi-temperature fit; a value comparable with these values. *FWHM*'s of the order of a few hundreds of km s^{-1} are also found by Günther & Schmitt based on *FUSE* observations, but in a wavelength area around 1000 Å and based on cooler ions. Their broadening might originate from other processes and not directly be linked to the broadening in the X-ray spectrum.

The last column shows the observed line photon fluxes as measured at Earth in units 10^{-6} photons cm^{-2} s^{-1}. The lines of H-like neon, oxygen, nitrogen, and carbon are strong, as well as He-like lines of neon and oxygen. For these lines the uncertainties of the flux values are of the order of 10%. The iron lines are moderately strong. Especially for neon and oxygen higher Rydberg states are visible up to n = 5. Their relative uncertainties are higher.

4.1. Emission measures from individual line fluxes

Line fluxes (F), emission measure (EM), and abundances (A) are related to each other by means of the formula:

$$F = (4.1807 \times 10^{-54} \times \lambda \times A \times EM \times 10^{-s})/{\rm d}p^2.$$

In this formula F is the line flux in units of photons cm^{-2} s^{-1}, λ is the wavelength of the line in Å, A is the abundance relative to solar photospheric values, EM is the emission measure in units cm^{-3}, dp is the distance of the source in parsecs and s is the emissivity factor given by Mewe et al. (1985), applied for the temperature ($T_{\rm m}$) of maximum emissivity. In Table 4 the values of the quantity $A \times EM$ obtained from individual line fluxes are given. The given uncertainties in this quantity are based on the uncertainties of the measured line fluxes and an assumed average uncertainty of 15% in the theoretical transition probabilities of the lines. The latter value might be a bit low for weak lines and a bit too high for strong resonance transitions. Since the forbidden and intercombination lines in He-like ions behave as communicating tubes under influence of the density I have used the sum (f+i) in this table.

From the table we notice that the value of $A \times EM$ differ up to a factor of 10. For comparable values of $T_{\rm m}$ the values of EM, however, should be the same. The difference in value of $A \times EM$ in these cases is caused by deviations from solar abundance values for the involved ions. As an example: the ions O VII and N VII, although appearing in the same temperature range, show a difference of a factor 3 in the values of $A \times EM$. This indicates an overabundance of nitrogen compared to oxygen by a factor of about 3. The same way (based on O VIII and Ne IX), an overabundance of neon compared to oxygen is established by a factor of about 10. Absolute values of the abundances are difficult to determine on the basis of line fluxes, since they are anti-correlated with the emission measure. $A \times EM$ is a robust quantity.

Table 4. Calculated values of $A \times EM$, based on individual line fluxes.

Ion	λ_0 [Å]	Flux	log $T_{\rm m}$	s	$A \times EM$ cm^{-3}
Si XIV	6.182	3.9(2.3)	7.22	1.58	1.66(1.01)
Si XIII	6.648	3.4(2.2)	7.00	1.64	1.54(1.02)
Si XIII	f+i	5.1(3.1)	7.00	1.77	3.09(1.93)
Mg XII	8.423	4.2(—-)	7.00	1.86	2.49(—-)
Mg XI	9.169	6.4(3.4)	6.81	1.70	2.41(1.33)
Mg XI	9.314	12.0(6.2)	6.81	1.79	5.47(2.94)
Ne X	9.708	7.6(4.8)	6.79	2.70	27.1(17.6)
Ne X	10.239	11.5(4.5)	6.78	2.10	9.79(4.10)
Ne IX	10.765	7.7(3.7)	6.60	2.95	44.00(22.1)
Ne IX	11.001	12.6(4.2)	6.60	2.61	32.20(11.8)
Ne IX	11.544	22.0(4.8)	6.59	2.14	18.10(4.79)
Ne X	12.134	89.6(7.8)	6.77	1.18	7.71(1.34)
Ne IX	13.447	215.0(11.0)	6.59	1.31	22.50(3.57)
Ne IX	f+i	210.2(11.8)	6.59	1.36	24.40(3.90)
Fe XVII	15.013	35.9(6.5)	6.72	0.66	0.75(0.18)
O VIII	15.176	9.0(4.1)	6.51	2.09	5.03(2.41)
Fe XVII	15.260	17.4(5.1)	6.72	1.21	1.28(0.42)
O VIII	16.006	29.7(5.4)	6.50	1.48	3.86(0.91)
Fe XVII	16.775	20.4(4.6)	6.71	0.98	0.80(0.22)
Fe XVII	17.05+.10	38.0(16.3)	6.71	0.67	0.72(0.33)
O VII	18.627	17.5(6.7)	6.34	1.51	2.09(0.86)
O VIII	18.969	229.0(12.0)	6.48	0.52	2.76(0.44)
N VII	20.910	20.7(8.6)	6.34	2.47	20.10(8.88)
O VII	21.602	119.0(12.0)	6.33	0.64	1.66(0.30)
O VII	f+i	118.3(12.7)	6.32	0.69	1.81(0.33)
N VII	24.781	81.2(11.3)	6.32	1.48	6.83(1.40)
N VI	28.787	31.2(12.0)	6.17	1.67	3.50(1.44)
N VI	f+i	33.1(11.8)	6.16	1.70	3.93(1.52)
C VI	33.736	59.3(11.0)	6.13	0.94	1.06(0.25)

Notes: A is the elemental abundance and EM the emission measure. $T_{\rm m}$ and s are the temperature of maximum emissivity of the line and the corresponding line emissivity factor. λ_0 is the theoretical wavelength from Kelly (1987). Fluxes are given in units 10^{-6} photons cm^{-2} s^{-1}. $A \times EM$ is given in 10^{52} cm^{-3}. The error in $A \times EM$ includes the relative error in the flux values and a 15% error in the values for transition probabilities, imbedded in "s".

4.2. Comparison with observed line photon fluxes from other papers

In this subsection I compare the observed line photon fluxes obtained in this work with the most recent results from high-resolution X-ray spectroscopy, i.e., Stelzer & Schmitt (2004) using *RGS* aboard *XMM-Newton*, Kastner et al. (2002), and Ness & Schmitt (2005), applying *HETGS* aboard *Chandra* (see Table 5). The values given by Ness & Schmitt (2005) have been recalculated from energy fluxes to photon fluxes. For quite a number of lines the comparison is satisfactory, taking into account the uncertainties in the obtained fluxes. However, some severe deviations that exceed the given uncertainties are noticed. This is especially true for the comparison between the work of Stelzer & Schmitt (2004) and Kastner et al. (2002).

The deviations are not limited to weak lines with high uncertainties in their measured flux values, but they appear also for the strong Ne IX lines around 13.5 Å and the strong O VIII line

Table 5. Comparison of observed line photon fluxes.

ion	λ_0 [Å]	Flux this work	Flux Stelzer	Flux Kastner	Flux Ness
Si XIV	6.182	3.9(2.3)	—	2.7(1.9)	—
Si XIII	6.648	3.4(2.2)	—	2.1(1.7)	—
Si XIII	6.688	2.4(2.2)	—	0.8(1.2)	—
Si XIII	6.740	2.7(2.2)	—	1.4(1.4)	—
Si XIII	f+i	5.1(3.1)	—	2.2(1.8)	—
Mg XII	8.423	4.2(—-)	—	3.0(2.0)	—
Ne X	9.708	7.6(4.8)	—	2.0(2.1)	—
Ne X	10.239	11.5(4.5)	—	7.8(2.8)	11.2(1.8)
Ne IX	11.544	22.0(4.8)	—	18.0(4.6)	—
Ne X	12.134	89.6(7.8)	63(15)	73.7(7.8)	96.4(7.0)
Ne IX	13.447	215.0(11.0)	231(22)	122.4(11.9)	—
Ne IX	13.553	129.0(9.0)	174(11)	79.2(10.5)	—
Ne IX	13.700	81.2(7.7)	82(15)	35.3(8.6)	—
Ne IX	f+i	210.2(11.8)	256(19)	114.5(13.6)	—
Fe XVII	15.013	35.9(6.5)	—	$\lesssim$179.0	46.2(8.1)
O VIII	15.176	9.0(4.1)	—	$\lesssim$15.9	—
Fe XVII	15.260	17.4(5.1)	—	23.2(8.4)	29.0(5.4)
O VIII	16.006	29.7(5.4)	35(11)	35.7(10.4)	51.4(7.8)
Fe XVII	16.775	20.4(4.6)	—	15.3(9.9)	21.4(5.7)
Fe XVII	17.051	22.9(12.6)	27(9)	35.9(13.1)	52.9(9.0)
Fe XVII	17.100	15.1(10.3)	—	25.4(12.7)	30.3(6.9)
O VII	18.627	17.5(6.7)	17(4)	10.8(14.1)	—
O VIII	18.969	229.0(12.0)	304(28)	195.7(28.0)	284.5(26.5)
O VII	21.602	119.0(12.0)	174(21)	91.3(36.3)	—
O VII	21.804	103.0(11.0)	95(15)	105.4(40.4)	—
O VII	22.101	15.3(6.3)	4(6)	$\lesssim$57.0	—
O VII	f+i	118.3(12.7)	99(16)	$\lesssim$162	—
N VII	24.781	81.2(11.3)	118(22)	87.8(36.5)	—
N VI	28.787	31.2(12.0)	29(13)	—	—
N VI	29.084	27.1(10.0)	13(6)	—	—
N VI	29.536	6.0(6.0)	4(5)	—	—
N VI	f+i	33.1(11.7)	17(8)	—	—
C VI	33.736	59.3(11.0)	78(14)	—	—

Notes: This work, Stelzer & Schmitt (2004), Kastner et al. (2002), and Ness & Schmitt (2005). λ_0 is the theoretical wavelength from Kelly (1987). Flux in units 10^{-6} photons cm^{-2} s^{-1}.

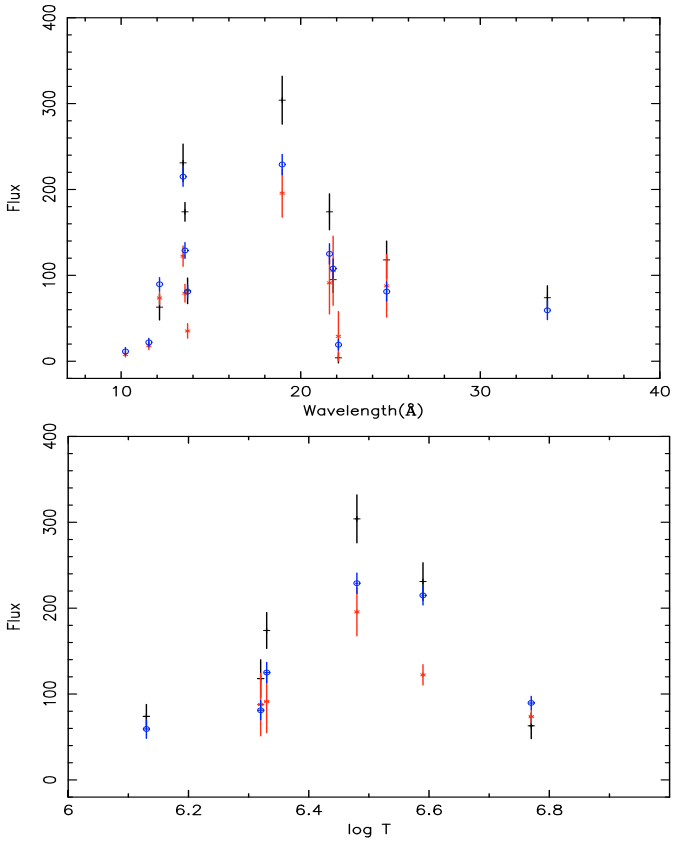

Fig. 3. Line fluxes versus wavelength (*top*) and versus log T (*bottom*) from: - Stelzer & Schmitt (2004), * Kastner et al. (2002) and ° This work (black, red, and blue in the electronic version, respectively). Fluxes are given in 10^{-6} photons cm^{-2} s^{-1}.

at 19.0 Å (see Fig. 3). These figures show the observed line photon fluxes measured by Stelzer & Schmitt (2004), Kastner et al. (2002), and this work versus wavelength and versus temperature of maximum emissivity of the line. From these figures it is difficult to conclude whether the differences are wavelength dependent, and therefore due to the use of three different instruments, or temperature dependent, and therefore related to variability of emission measures in the source TW Hya. The line ratios of the Ne IX lines, however, are comparable for the three spectra (see also the next section).

4.3. Temperature and density determination based on individual line flux ratios

The ratios between the line fluxes of the resonance lines from two ionisation stages of the same elements provide valuable information on the temperature regime of the plasma. Apart from that the line triplets in the He-like ions, consisting of a resonance line (r), an intercombination line (i) and a forbidden line (f), are strong diagnostic tools for temperature as well as for density (Gabriel & Jordan 1969).

4.3.1. Temperature

The temperature can be established, based on individual line fluxes. The ratio between the summed fluxes of the line triplets in the He-like ions and the resonance lines of H-like ions as well as the ratio (f+i)/r in the He-like line-triplets are temperature sensitive. As values for the ratios between the He-like line triplets and H-like resonance lines I obtain 0.79(.23) for N , 1.04(.09) for O , 4.74(.45) for Ne , and 2.2(1.6) for Si , resulting in temperatures of 0.180(.022) keV, 0.244(.007) keV, 0.296(.007) keV, and 1.13(0.50) keV, respectively. These results are based on tables of line-emissivities given by Mewe et al. (1985) and MEKAL. My ratio for O , as well as my $N_{\rm H}$ value are a bit higher than the values used by Güdel & Telleschi (2007) in their Fig. 2.

As ratios (f+i)/r in the He-like ions N VI, O VII, and Ne IX the values of 1.06(.55), 0.994(.146), and 0.978(.074) were established, respectively. These values correspond to temperatures of $\lesssim$0.28 keV, 0.129(.043) keV, and 0.18(.05) keV, as derived from tables given by Porquet et al. (2001). They all cover nicely the values obtained in the multi-T fit (Sect. 3.2).

4.3.2. Density

By definition (see Sect. 3.2), knowledge of the electron density $n_{\rm e}$ offers the possibility to derive the emitting volume, assuming a source with spatially constant $n_{\rm e}$.

The ratios (f/i) of C V, N VI, O VII, Ne IX, Mg XI, and Si XIII serve as density diagnostic. The line triplet of S XV is not

resolved and given as one feature in Table 3. Their lines are located in the range from 5 to 45 Å covered by *LETGS*. Here, I will focus on the ions N VI, O VII, and Ne IX. They are the stronger of the line triplets and well resolved.

Considering the measured line fluxes (see Table 3), the f/i ratios of N VI, O VII, and Ne IX are $\lesssim$.46, 0.15(.06) and 0.63(.07), respectively. These ratios result in densities of $\gtrsim 6.5 \times 10^{10}$ cm^{-3} for N VI, $n_e = 8.2(-2.4, +6.4) \times 10^{11}$ cm^{-3} for O VII, and of $n_e = 3.5(1.0) \times 10^{12}$ cm^{-3} for Ne IX (Porquet et al. 2001). This is in fair agreement with the values obtained from the multi-temperature fit (see Table 2).

5. Discussion

In this section I will discuss my results and pay special attention to differences and agreements between my results and results given in former publications. It is difficult to conclude where differences come from: whether they originate in the use of three different instruments or different models, in erroneous interpretations, or in actual variation of the source.

The three obtained CIE-temperatures (0.127(.012), 0.264(.007), and 1.45(.43) keV) are in very good agreement with values established by Stelzer & Schmitt (2004) (0.172, 0.272, and 1.72 keV, respectively) and by Robrade & Schmitt (2006) (0.24, 0.60, and 1.37 keV, respectively). To improve the shape op the continuum a blackbody component of 0.187(.016) keV was introduced that replaces the temperature bin of 0.60 keV found by Robrade & Schmitt. From Table 2 in Günther et al. (2007) we notice that this CIE temperature component (0.72 keV) is not very significant. The introduction of my blackbody component models the shape of the continuum from 5 to 15 Å better. Thanks to that it offers the possibility to fit some weak line features of silicon and sulphur properly. It reduces χ^2 significantly; from 537 (applying parameters given by Robrade & Schmitt 2006) to 334 (this work) for 299 degrees of freedom and just covering the wavelength range from 5 to 35 Å. It is possible that my "blackbody" continuum describes a continuum formed by many weak lines not present in the databases.

My fitted value of N_H is higher than the values given by Stelzer & Schmitt (2004) and Robrade & Schmitt (2006). This higher value is necessary to suppress the appearance of lines above 40 Å in the model that are absent in the data. A fit with a Gaussian at the theoretical position of the Si XII lines at 44 Å (where no feature is visible) yields an upper limit of $7{\times}10^{-6}$ photons cm^{-2} s^{-1}. These lines also appear in the model when using the parameter sets given by Stelzer & Schmitt (2004) and Robrade & Schmitt (2006), based on *RGS*, to describe the *LETGS* spectrum. Their parameters, however, were based on data sets limited to 35 Å, not covering the higher wavelength range where these lines are located.

The abundance pattern (*A*/O) is quite well the same as for the two other papers, especially concerning the Model B in Stelzer & Schmitt (2004). Neon and nitrogen are enhanced. My carbon abundance relative to oxygen is a bit higher than theirs, but that is due to my higher N_H value. My absolute abundance values, however, are far higher (by a factor 2–3) than those given in the two other papers. This results in correspondingly lower values of the emission measures, as the quantity $A \times EM$ is robust. Despite the big difference in absolute values for the emission measure the overall emission measure shape agrees with Stelzer & Schmitt (2004) and the quantity $A \times EM$ is comparable for the three papers (Stelzer & Schmitt 2004; Robrade & Schmitt 2006; and this work).

The electron density n_e, derived from O VII and Ne IX is high compared to electron densities observed in stellar coronae. My obtained n_e value of about 10^{12} cm^{-3} corresponds to values given in the other papers. It is related to the temperature regime around .2 keV and considered to be an indication for a process of accretion.

Although the overall pattern of the line fluxes and line flux ratios agree with Stelzer & Schmitt (2004) and Kastner et al. (2002) it is wondering that even for strong features the absolute line flux values differ considerably. This is especially true for the line fluxes given by Stelzer & Schmitt (2004) and Kastner et al. (2002). Thanks to the fact that the ratios agree better than the absolute values the conclusions drawn concerning the density, temperatures, and abundances are the same for the three papers. The underlying reason for the difference in line flux might be related to the use of different instruments or to the variability of the source, due to higher volumes of accreted material. The latter is suggested by the difference in line fluxes of Ne X and Ne IX. The ratio (f+i)/r in He-like ions is close to 1, indicating a plasma in collisional equilibrium.

The measured line positions are slightly shifted to higher wavelength. The corresponding velocity of about 30 km s^{-1} is higher than the satellite motion or v_{rad} of TW Hya. The lines are broadened, in addition to the instrumental LSF, by an *FWHM* of ~0.025 Å. This is broader than comparable lines in the coronal spectrum of Capella. Shift and broadening might be fingerprints of the velocities in the funneling accreted plasma from the disc to the stellar surface, although a calibration bias cannot be ruled out. In the latter case it might affect *LETGS* as well as *RGS*.

6. Summary

The overall conclusions based on the *LETGS* spectrum of TW Hya confirm the statements made by Robrade & Schmitt (2006), Stelzer & Schmitt (2004) and Kastner et al. (2002), concerning the dominance of a high density plasma ($n_e \simeq 10^{12}$ cm^{-3}) at temperatures of about 0.2 keV. This is different from coronal cool star spectra for which higher temperatures and lower densities are determined (e.g., Raassen et al. 2003).

The abundances of neon (10×) and nitrogen (3×) are strongly enhanced in comparison with the oxygen abundance.

Thanks to the extended wavelength region of *LETGS* more information about the spectrum above 40 Å was obtained, resulting in a somewhat higher value of the N_H, i.e., the sum of the interstellar absorption and the circumstellar absorption just near TW Hya, compared to values used or obtained by Stelzer & Schmitt (2004) and Robrade & Schmitt (2006).

Differences in line fluxes between the papers Stelzer & Schmitt (2004), Kastner et al. (2002), Ness & Schmitt (2005) and this work are an indication for variability in mass accretion rate, but might also be due to instrumental differences.

An additional blackbody component is added to improve the multi-temperature fit and to describe a deficiency in continuum radiation between 5 and 15 Å in the model.

Acknowledgements. The SRON National Institute for Space Research is supported financially by NWO.

References

Anders, E., & Grevesse N. 1989, Geochim. Cosmochim. Acta, 53, 197
Arnaud, M., & Rothenflug, R. 1985, A&AS, 60, 425

Feigelson, E. D., & DeCampli, W. M. 1981, ApJ, 243, L89
Feigelson, E. D., Casanova, S., Montmerle, T., & Guibert, J. 1993, ApJ, 416, 623
Gabriel, A. H., & Jordan, C., 1969, MNRAS, 145, 241
Grevesse, N., & Sauval, A.J. 1999, A&A, 347, 348
Güdel, M., & Telleschi, A. 2007, A&A, 474, L25
Günther, H. M., & Schmitt, J. H. M. M. 2008, A&A, 481, 735
Günther, H. M., Schmitt, J. H. M. M., Robrade, J., & Liefke, C. 2007, A&A, 466, 1121
Herbst, W., & Koret, D.L. 1988, AJ, 96, 1949
Huélamo, N., Figueira, P., Bonfils, X., et al. 2008, A&A, 489, L9
Kaastra, J. S., Mewe, R., & Nieuwenhuijzen H. 1996a, in UV and X-ray Spectroscopy of Astrophysical and Laboratory Plasmas, ed. K. Yamashita, & T. Watanabe (Universal: Academy Press, Inc., Tokyo), 411 (SPEX)
Kaastra, J. S., Mewe R., Liedahl, D. A., et al. 1996b, A&A, 314, 547
Kastner, J. H., Huenemoerder, D. P., Schulz, N. S., et al. 2002, ApJ, 567, 434
Kelly, R. L. 1987, J. Phys. Chem. Rev. Data, 16
Mekkaden, M. V. 1998, A&A, 340, 135
Mewe, R., Gronenschild, E. H. B. M., & van den Oord, G. H. J. 1985, A&AS, 62, 197
Mewe, R., Kaastra, J. S., & Liedahl, D. A. 1995, Legacy, 6, 16 (MEKAL)
Ness, J.-U., & Schmitt, J. H. M. M. 2005, A&A, 444, L41
Perryman, M. A. C., Lindegren, L., Kovalevsky, J., et al. 1997a, A&A, 323, L49
Perryman, M. A. C. 1997b, The Hipparcos and Tycho Catalogues, ESA SP-series, 1200
Porquet, D., Mewe, R., Dubau. J., et al. 2001, A&A, 376, 1113
Raassen, A. J. J., Mewe R., Audard M., & Güdel, M. 2003, A&A, 411, 509
Reid, N. 2003, MNRAS, 342, 837
Robrade, J., & Schmitt, J. H. M. M. 2006, A&A, 449, 737
Rucinski, S. M., Matthews, J. M., Kuschnig, R., et al. 2008, MNRAS, 391, 1913
Setiawan, J., Henning, Th., Launhardt, R., et al. 2008, Nature, 451,38
Stelzer, B., & Schmitt, J. H. M. M. 2004, A&A, 418, 687
van Leeuwen, F. 2007, A&A, 474, 653